Article ID: 1006-8775(2019) 02-0245-12

TOPOGRAPHY–DEPENDENT HORIZONTAL LOCALIZATION SCALE SCHEME IN GRAPES–MESO HYBRID EN–3DVAR ASSIMILATION SYSTEM

XIA Yu (夏 宇)[1], CHEN Jing (陈 静)[2], ZHI Xie-fei (智协飞)[1], ZHUANG Zhao-rong (庄照荣)[2], CHEN Liang-lv (陈良吕)[3], WANG Jing-zhuo (王婧卓)[3]
(1. Nanjing University of Information Science & Technology, Nanjing 210044 China;
2. Numerical Weather Prediction Center, China Meteorological Administration, Beijing 100081 China;
3. Chinese Academy of Meteorological Sciences, Beijing 100081 China)

Abstract: Based on the GRAPES-MESO hybrid En-3DVAR (Ensemble three-dimension hybrid data assimilation for Global/Regional Assimilation and Prediction system) constructed by China Meteorological Administration, a 7-day simulation (from 10 July 2015 to 16 July 2015) is conducted for horizontal localization scales. 48h forecasts have been designed for each test, and seven different horizontal localization scales of 250, 500, 750, 1000, 1250, 1500 and 1750 km are set. The 7-day simulation results show that the optimal horizontal localization scales over the Tibetan Plateau and the plain area are 1500 km and 1000 km, respectively. As a result, based on the GRAPES-MESO hybrid En-3DVAR, a topography-dependent horizontal localization scale scheme (hereinafter referred to as GRAPES-MESO hybrid En-3DVAR-TD-HLS) has been constructed. The data assimilation and forecast experiments have been implemented by GRAPES-MESO hybrid En-3DVAR, 3DVAR and GRAPES-MESO hybrid En-3DVAR-TD-HLS, and then the analysis and forecast field of these three systems are compared. The results show that the analysis field and forecast field within 30h of GRAPES-MESO hybrid En-3DVAR-TD-HLS are better than those of the other two data assimilation systems. Particularly in the analysis field, the root mean square error (RMSE) of u_wind and v_wind in the entire vertical levels is significantly less than that of the other two systems. The time series of total RMSE indicate, in the 6-30h forecast range, that the forecast result of En-3DVAR-TD-HLS is better than that of the other two systems, but the En-3DVAR and 3DVAR are equivalent in terms of their forecast skills. The 36-48h forecasts of three data assimilation systems have similar forecast skill.

Key words: GRAPES-MESO; hybrid En-3DVAR data assimilation; topography-dependent; horizontal localization scales

CLC number: P457.8 **Document code:** A

doi: 10.16555/j.1006-8775.2019.02.010

1 INTRODUCTION

In current research and practice, the main methods of data assimilation are three dimensional variational data assimilation (hereinafter referred to as 3DVAR) (Parrish and Derber[1]; Rabier et al.[2]; Barker et al.[3]) and Ensemble Kalman Filter data assimilation (hereinafter referred to as EnKF) (Anderson[4]; Whitaker and Hamil[5]; Snyder and Zhang[6]; Tong and Xue[7]; Zhang et al.[8]; Torn et al.[9]; Meng and Zhang[10]; Zhang et al.[11]). They both have advantages and disadvantages. 3DVAR breaks the limit of liner relationship between observational variables and analysis variables compared to previous methods, making it possible to use a variety of unconventional observations (radar and satellite, etc.) to improve the quality of numerical predictions. However, it usually uses climate-statistics-based, uniform, and isotropic background error covariance information, which ignores the stream-dependent properties of background error covariance. It cannot accurately describe the forecast errors when weather situation changes. EnKF uses the Monte-Carlo sampling method to obtain ensemble forecasts to get the stream-dependent background error covariance. It uses the optimal estimation method to update ensemble forecast, and then evolves the covariance of the stream-dependent background errors over time by the ensemble forecast perturbation. Although this method has advantages over 3DVAR, it computational cost is higher. Therefore, some scientists proposed a new method–hybrid data assimilation method, which combines the advantages of these two methods.

In the recent decade, hybrid data assimilation has become a widely-researched topic (Hamill et al.[12]; Wang[13-16]; Wang et al.[17]; Clayton et al.[18]; Courtier et al.[19]; Buehner[20]; Wang et al.[21]) in the data assimilation field. It has achieved some encouraging results and promises future research potential. Many researchers have already done a great deal of work based on hybrid

Received 2018-01-30; **Revised** 2019-03-05; **Accepted** 2019-05-15

Foundation item: National Natural Science Foundation of China (91437113, 41605082)

Biography: XIA Yu, Ph.D. Candidate, Associate Researcher, primarily undertaking research on numerical simulation.

Corresponding author: CHEN Jing, e-mail: chenj@cma.gov.cn

3DVAR data assimilation. Using the low-resolution quasi-geostrophic model, Hamill, Snyder and Whitaker coupled the covariance of climatic statistical background error and the covariance of ensemble estimated background error through a linear combination method, for the first time to construct an EnKF-3DVAR hybrid data assimilation system[22-24]. In 2003, Lorenc discussed how to apply the ensemble estimate background error covariance to the 3DVAR frame by extending control variable method[25]. In 2005, Buehner further discussed how to apply the ensemble estimation background error covariance to the 3DVAR framework by extending control variable method[26]. In 2007, Wang et al. proved that extending control variable method and linear combination method are theoretically equivalent[27]. At the same time, hybrid data assimilation schemes based on four-dimensional variances have also been greatly developed (Liu et al.[28-29]; Buehner et al.[30-31]). In recent years, research on the hybrid data assimilation has won great scholar attention in China (Ma et al.[32-33]; Zhang et al.[34]; Zhu et al.[35]; Shen et al.[36]). Chen et al.[37] utilized GRAPES-MESO 3DVAR data assimilation system and GRAPES-MESO ensemble forecasting system (Chen et al.[37]; Zhang et al.[38-40]) to construct GRAPES-MESO hybrid En-3DVAR data assimilation system and conducted some experiments. The experimental results showed that when the ensemble estimation background error covariance is introduced to the GRAPES-MESO 3DVAR system, the quality of data assimilation in the analysis field and forecast field of GRAPES-MESO system can be improved, with more obvious improvements in areas with sparse observations.

EnKF usually uses fewer members to estimate ensemble background error covariance, which will produce abnormal correlations when the distance between these two grids are relatively far away. It underestimates the background error covariance, and weakens the effect of the observations, eventually leads to filter diverging. This is due to the sampling error of ensemble forecast. Houtekamer and Mitchell first discovered that the result of EnKF can be improved without using long-range grids observations[41]. Therefore, localizing the ensemble background error covariance is the main method to solve this problem. Houtekamer and Mitchell used "Schur product" and a distance-dependent function when estimating the ensemble covariance, and found that there was a significant improvement in analysis errors[42]. Gaspari and Cohn discussed how covariance localization improved the ensemble analysis[43]. Ott et al. proposed and improved LEKF (Local Ensemble Kalman Filter) localization scheme[44-45]. Hunt et al. proposed the LETKF (Local Ensemble Transform Kalman Filter) scheme[46] based on the work of Ott et al.[44-45], which improved the computational efficiency. Miyoshi et al. pointed out that LETKF can be more flexible than LEKF in choosing observations[47]. Szunyogh et al. used a parallel GIS (Geographic Information System) system to test the accuracy and computational efficiency of LETKF[48]. There are relatively few studies on the covariance localization in China (Liu and Min[49]). China is a country with complex terrain. The sparse observation data and special terrain over the Tibetan Plateau have seriously affected the quality of data assimilation in these areas. Besides, in the data assimilation system, the horizontal localization scale is an important parameter which determines the transmission distance of the observation information. Therefore, the horizontal localization scales in the Tibetan Plateau should not be the same as the plains, which have more intensive observations.

In this paper, based on GRAPES-MESO hybrid En-3DVAR data assimilation system constructed by China Meteorological Administration, the 7-day simulations have been implemented to verify the optimal horizontal localization scales between Tibetan Plateau and plains in the forecast area. Based on the results of the 7-day simulations, we designed and constructed a topography-dependent horizontal localization scales method (only for ensemble background error covariance) based on GRAPES-MESO hybrid En-3DVAR data assimilation system (GRAPES-MESO hybrid En-3DVAR-TD-HLS), and then compared the improvement over GRAPES-MESO hybrid En-3DVAR and GRAPES-MESO 3DVAR systems. In this paper, only radiosonde, surface observations and ship observations were assimilated in those experiments. The spatial distribution of these observations is shown in Fig. 1.

Section 2 details the GRAPES-MESO hybrid En-3DVAR and GRAPES-MESO-TD-HLS hybrid En-3DVAR data assimilation system. The experiment designs are presented in section 3, and the results of cycled En-3DVAR, 3DVAR, and En-3DVAR-TD-HLS approach are presented in section 4. Conclusions are given in section 5.

2 THE GRAPES–MESO HYBRID EN–3DVAR–TD–HLS

2.1 *GRAPES –MESO hybird En –3DVAR data assimilation system*

The GRAPES-MESO hybrid En-3DVAR data assimilation system (resolution: 0.15°×0.15°) is cycled with time as shown in Fig. 2, with each cycle consisting of the following steps:

1) The ensemble forecasting perturbations are updated from GRAPES-MESO ETKF system by a 12h forecast with 14 ensemble members, and then ensemble background error covariance are generated by the ensemble forecasting perturbations through extended control variable method[18]. The generation of ensemble background error covariance is as follows:

$$x_k^e = (x_k - \bar{x})/\sqrt{K-1} \tag{1}$$

$$P_e^f = \sum_{k=1}^{K} x_k^e (x_k^e)^T \tag{2}$$

where x_k^e is the normalized ensemble perturbation which

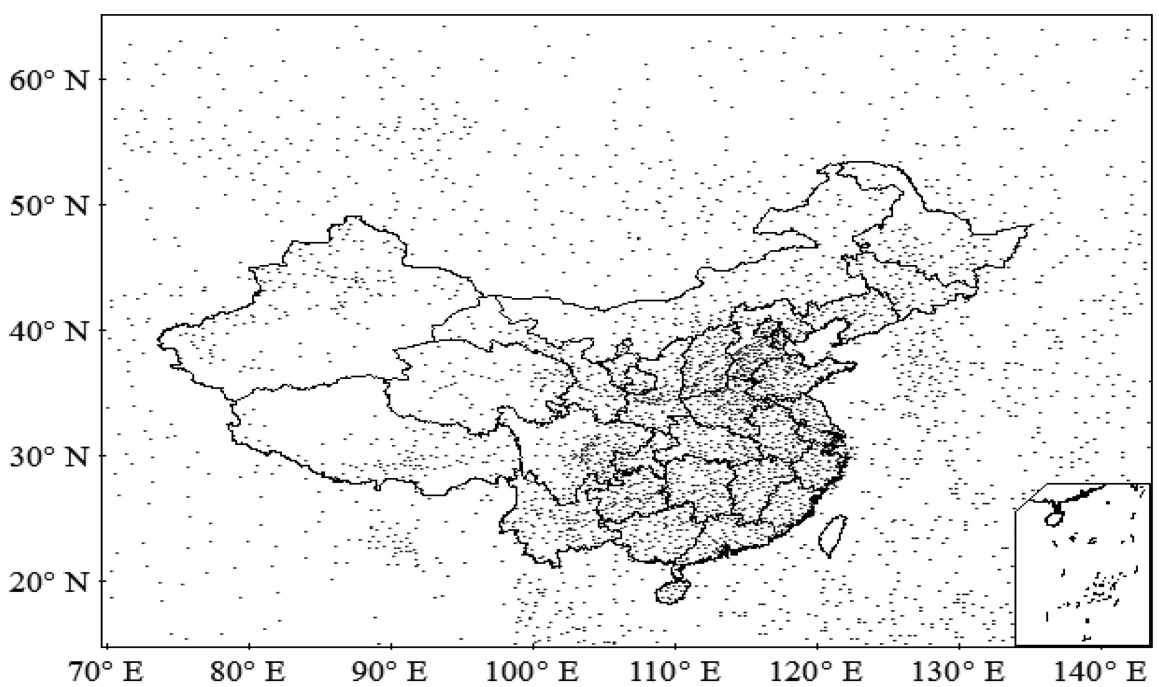

Figure 1. The spatial distribution of the observations. Solid point for surface observation, hollow cycle for radiosonde and plus for ships.

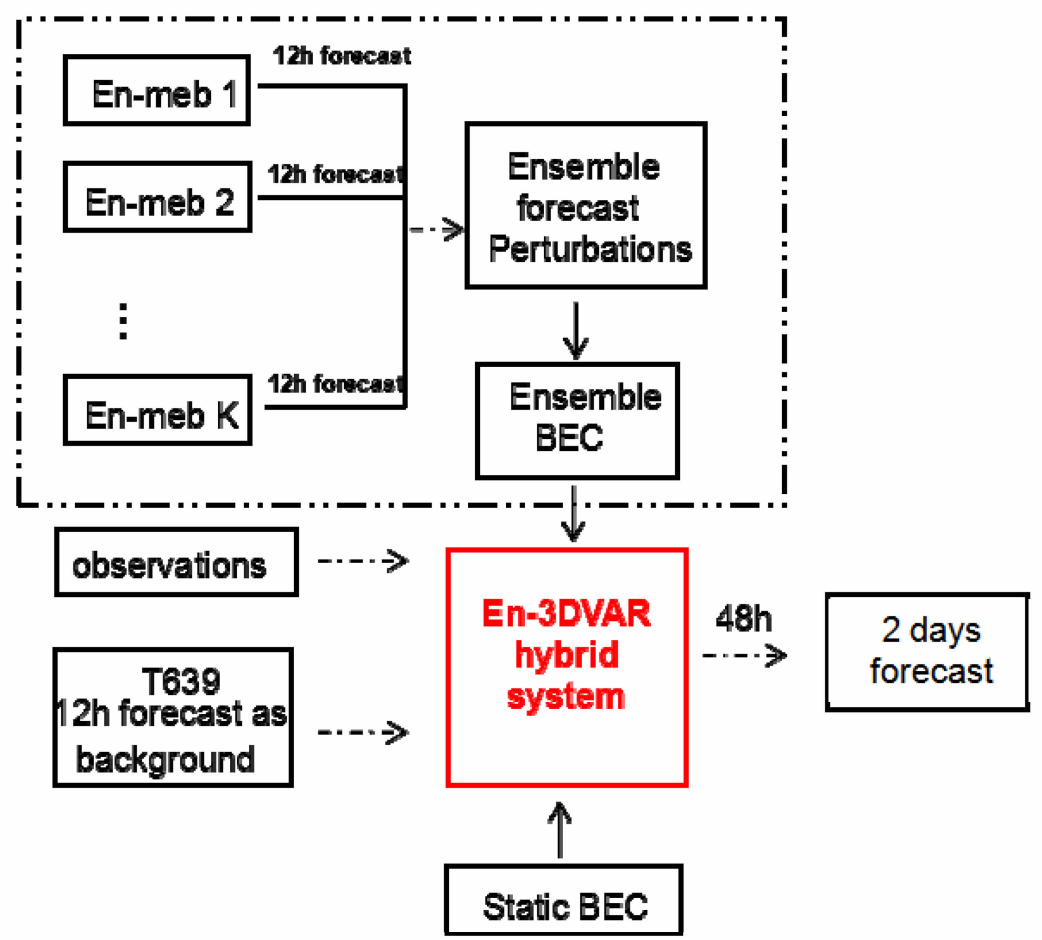

Figure 2. Schematic diagram of the GRAPES-MESO hybrid En-3DVAR analysis-forecast cycle.

is taken from the 12h forecast of GRAPES-MESO ETKF system, x_k is the kth ensemble forecast, $\bar{x}$ is the ensemble mean, K is the ensemble size, and P_e^f is the ensemble background error covariance.

Because of the limited ensemble size, the ensemble background error covariance is low rank, and will lead to unreasonable correlation between variables in practical application [37]; therefore, we need to localize the P_e^f as follows:

$$B_e = P_e^f oC = \sum_{k=1}^{K} (x_k^e (x_k^e)^T) oC \quad (3)$$

where C is the localization matrix whose size is equal to P_e^f, o is the Schur product.

2) The static background error covariance is provided by the NMC method.

3) The boundary conditions and background data are generated by the global 12h forecasts of T639.

4) The data from 1) and 2) are combined with observational data, and then a 48h data assimilation and forecast experiment is conducted by using hybrid En-3DVAR system.

2.2 *Theoretical formula*

The hybrid data assimilation scheme can be achieved by using the method of extending control variables to combine the ensemble estimated and climate-statistics-based background error covariance. The cost function can be explained as follows:

where x' is the analysis increment, B_c and B_e are defined

$$J(x') = \frac{1}{2}(x')^T(\beta_c B_c + \beta_e B_e)^{-1}(x') + \frac{1}{2}(Hx'+d)^T R^{-1}(Hx'+d) \quad (4)$$

as climate-statistics-based and ensemble-estimate background error covariance, respectively. H is the operator mapping the model space to the observation space, and $d=H(xb)-y$ denotes the innovation vector. β_c and β_e are two factors defined as the weights of climate-statistics-based and ensemble-estimate background with the following relationship:

$$\beta_e^2 + \beta_c^2 = 1 \quad (5)$$

The state variables are velocity potential, stream function, humidity variable (relative humidity or specific humidity) and dimensionless pressure in these three data assimilation systems. Except for humidity variable (because the humidity field has too much uncertainty in GRAPES), the remaining state variables use the same horizontal localization scale in this paper. For mathematical details of the GRAPES-MESO based hybrid En-3DVAR system, readers can refer to Chen et al.[37].

2.3 *The GRAPES-MESO-TD-HLS hybrid data assimilation system*

The horizontal localization scale in the GRAPES-MESO En-3DVAR system is the same throughout the three-dimensional grid space of the experiment area, but some experiments found that the optimal horizontal localization scales are different between complex terrain areas (such as the Tibetan Plateau) and plain areas. Therefore, this paper selected e-index function as the basic function, and constructed a topography-dependent horizontal localization scales scheme (it does not change with the vertical level). The concrete realization is as follows:

$$e\_index(i,j) = e^{-(Z\max - zz(i,j))/\sigma^2} \quad (6)$$

$$Loc(i,j) = e\_index(i,j) * L \quad (7)$$

where Zmax is the highest point of the terrain (this paper uses 5500m as Zmax), $zz(i,j)$ is the height of the terrain at grid (i,j), σ is the morphological index, and the value of e_index ranges from 0 to 1. L is the default localization scale of the original system (GRAPES-MESO 3DVAR and GRAPES-MESO hybrid En-3DVAR).

$Loc(i,j)$ is the new horizontal localization scale at the grid (i,j) after the TD-HLS method. The value of $e\_index(i,j)$ can be obtained by Zmax, $zz(i,j)$ and σ. As a result, different horizontal localization scales on different grids can be achieved.

Figure 3 is the curve of e_index graphed against the height of the terrain under different morphological index (the values of the morphological indexes are 100, 150, 200 and 250). With the same σ, the e_index decreases as terrain height decreases. When σ is smaller, e_index decreases at a higher rate.

3 EXPERIMENT DESIGN

3.1 *The 7-day simulations of horizontal localization scale*

To explore the impact of horizontal localization scale on GRAPES-MESO hybrid En-3DVAR data assimilation system under different topographical conditions, we conducted a test over the Tibetan Plateau (70°E to 105°E, 25°N to 40°N) and the plain area (105°E to 145°E, 15°N to 40°N). The test lasted for 7 days from 10 July 2015 to 16 July 2015. We set seven different horizontal localization scales of 250, 500, 750, 1,000, 1,250, 1,500 and 1,750 km, and then ran the GRAPES-MESO hybrid En-3DVAR data assimilation system and calculated the total RMSE (7-day average) of the analysis and forecast fields in these two areas. The T639 (resolution 0.28125°×0.28125°) analysis data were used as the real atmospheric state to verify these 7 days simulations' result.

3.2 *Data assimilation and forecast experiments by three systems*

The experiment of data assimilation and 48h forecasts which began at 0000 UTC 12 Jun 2015 was carried out by 3DVAR, GRAPES-MESO En-3DVAR, and GRAPES-MESO En-3DVAR-TD-HLS. The details are described in Table 1. The forecast domain is 15°N

to 64.35°N, 70°E to 145.15°E, and resolution is 0.15°× 0.15°. The 12h forecast of the T639 global prediction system was used as background fields. The lateral boundary conditions were also provided by T639 global prediction system. Only conventional observations (surface observation, radiosonde and ships) were used in these experiments. The T639 (resolution 0.28125° × 0.28125°) analysis data were used as the real atmospheric state to verify these three systems' data assimilation and forecast results. The GRAPES-MESO En-3DVAR contains the Betts-Miller-Janjic cumulus convection parameterization scheme, the MRF planetary boundary layer parameterization scheme, the Noah land surface process parameterization scheme, the Monin-Obukhov planetary boundary layer parameterization scheme, the Dudhia short-wave radiation parameterization scheme, the RRTM long-wave radiation parameterization scheme, and the WSM6 micro-physical process parameterization scheme.

4 EXPERIMENT RESULTS

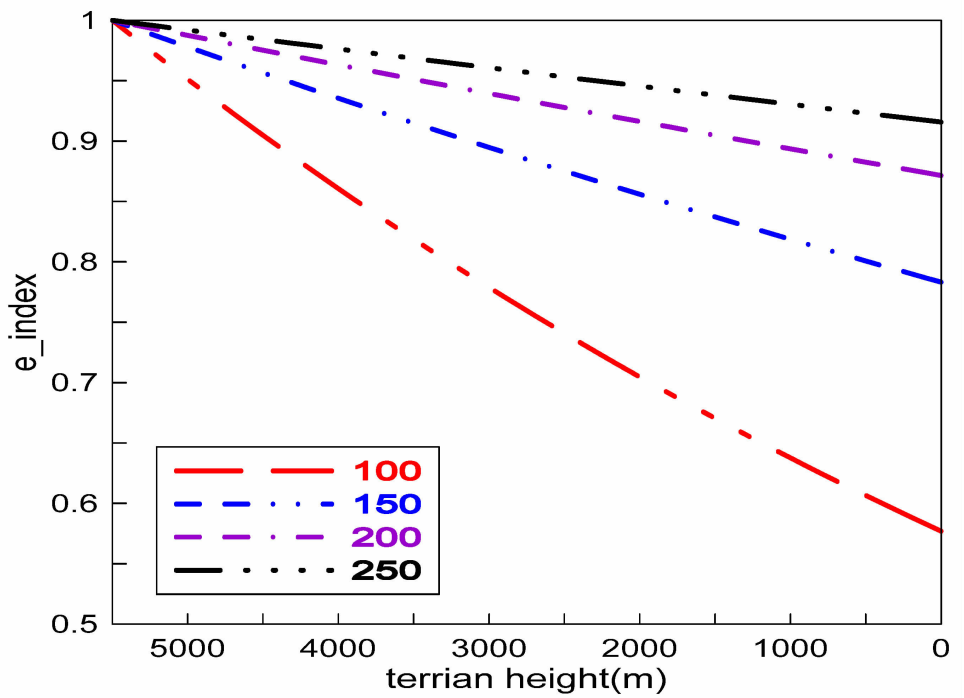

Figure 3. The curve of *e_index* changed with the height of the terrain which under different morphological index (the morphological indexes are 100, 150, 200 and 250).

Table 1. Details of three data assimilation experiments.

Name	β_c and β_e	scheme
3DVAR	none	The conventional observations are assimilated via GRPES-MESO 3DVAR system. The static background covariance is re-calculated via NMC method. The 12h forecast of the T639 global prediction system was used as background fields.
En-3DVAR	β_c=0.5 and β_e=0.5	Compared to the 3DVAR,the ensemble covariance was added to the 3DVAR frame by extending control variable method, and the other options are the same as 3DVAR.
En-3DVAR-TD-HLS	β_c=0.5 and β_e=0.5	The same as En-3dvar,but with TD-HLS method.

4.1 *The result of 7–day simulations*

Figure 4 shows the total RMSE (7-day average from 10 to 16 June 2015) of u_winds and and v_winds over the plain and the Tibetan Plateau. As can be seen from Fig. 3, when the horizontal localization scale is 1500 km, the RMSE of u_wind and v_wind over the Tibetan Plateau is the smallest. Compared to the Tibetan Plateau, the optimal horizontal localization scale over the plain is 1,000 km, the temperature and height are insensitive to horizontal localization scale, so we will not discuss them in details. This shows that under different topographic conditions, the optimal horizontal localization scale is different. In GRAPES-MESO En-3DVAR system, the horizontal localization scales in

the three-dimensional grid space have the same value, which is not consistent with the results of the 7-day simulations. Therefore, this paper constructed the topography-dependent horizontal localization scale method, which is based on the GRAPES-MESO hybrid En-3DVAR data assimilation system (GRAPES-MESO hybrid En-3DVAR-TD-HLS). As the optimal horizontal localization scales of the Tibetan Plateau and the plain area is 1,500 km and 1,000 km respectively, we set L (in formula 4) to 1,500 km. Corresponding to Fig. 2, when σ is equal to 100, the horizontal localization scale over the plain area is about 1,000 km. This setting is consistent with the results of 7-day simulations.

Figure 5 is the horizontal distribution of $Loc(i, j)$ under different terrain (σ equal to 100). As can be seen, the higher the terrain, the larger the horizontal localization scale. Over the plain area, the horizontal localization scale is about 1,000 km, and over the Tibetan Plateau the scale it is about 1,500 km. When the terrain is steeper, the horizontal localization scale becomes larger. It is consistent with the 7-day simulations result. Thus the σ used in the following experiments is 100.

4.2 *Data assimilation and forecast results of the three systems*

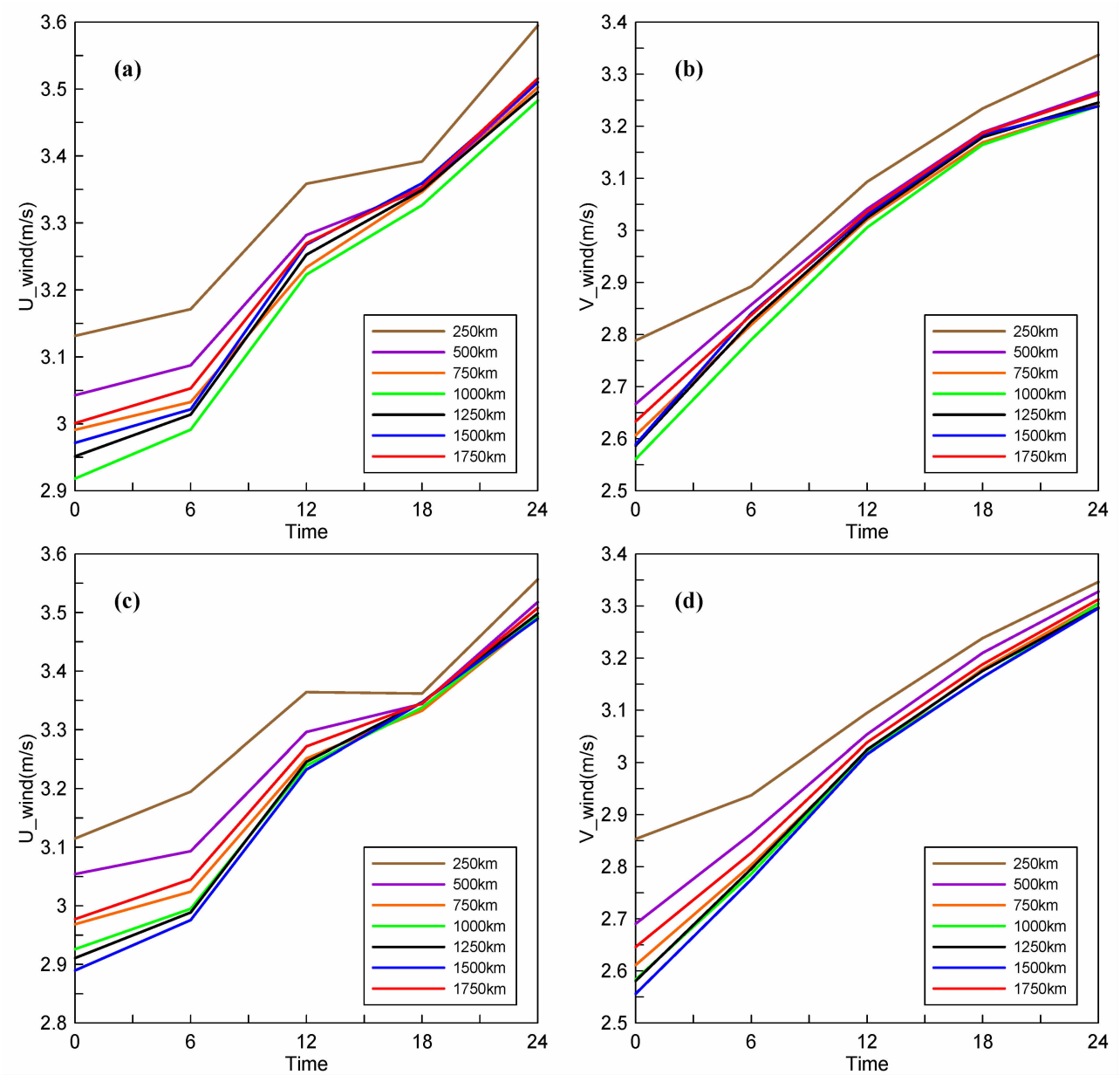

Figure 4. Time series of total RMSE of 7 days simulations with different horizontal localization scale for (a) u_wind over the plain, (b) v_wind over the plain , (c) u_wind over the Tibetan Plateau, and (d) v_wind over the Tibetan Plateau.

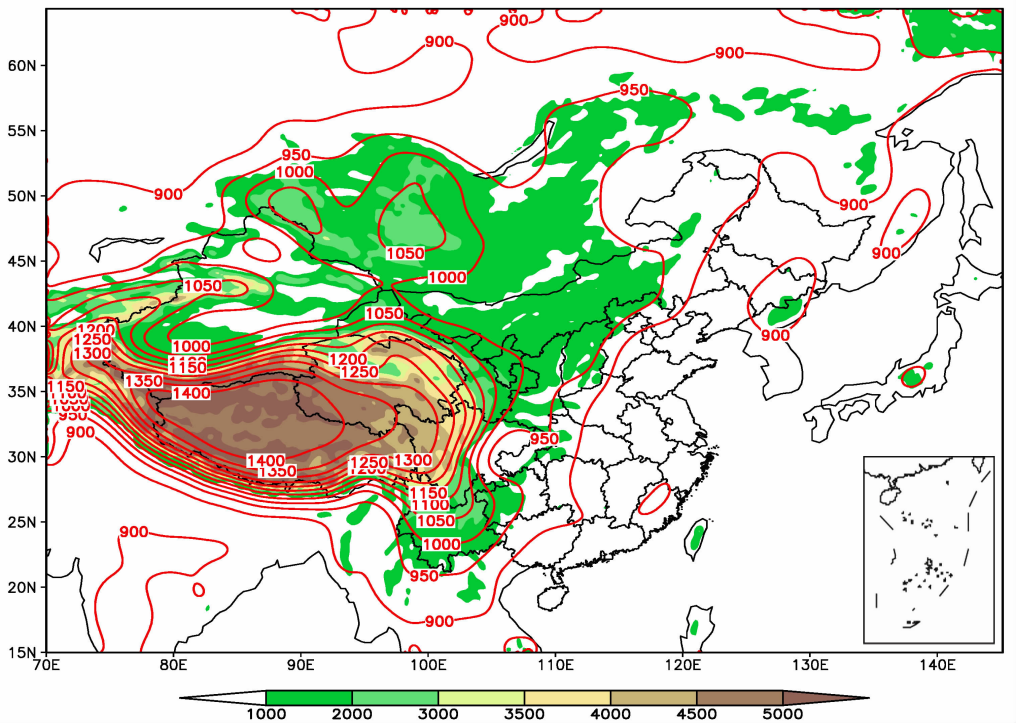

Figure 5. Horizontal distribution of $Loc(i, j)$ over different terrain. σ is equal to 100. The shaded region highlights the height of the terrain and the contours highlight the horizontal localization scale.

To verify the result of GRAPES-MESO En-3DVAR-TD-HLS, the data assimilation and forecast experiments have been conducted by using 3DVAR, GRAPES-MESO En-3DVAR, and GRAPES-MESO En-3DVAR-TD-HLS. Fig. 6 shows the results of the horizontal analysis increment of u_wind with one single-point pressure observation experiment, the point is at the plain (42°N, 117°E) and Tibetan plateau (35°N, 90° E) with the model level of 13. Fig. 6a and 6b represents the single-point pressure observation experiment over the plain, and we can see that the shape and structure of the u_wind analysis increment for En-3DVAR-TD-HLS and En-3DVAR are roughly the same. However, the range of u_wind analysis increment of GRAPES-MESO En-3DVAR-TD-HLS system is significantly less than that of GRAPES-MESO En-3DVAR, with the value in the center significantly greater than the latter. This means that the transmission distance of observational information by GRAPES-MESO En-3DVAR-TD-HLS over the plain area is smaller than that of GRAPES-MESO En-3DVAR, which can better reflect small and medium weather systems. The u_wind analysis increment of GRAPES-MESO En-3DVAR-TD-HLS is also smoother than that of the GRAPES-MESO En-3DVAR: the small perturbation of u_wind analysis increment is significantly less than that of GRAPES-MESO En-3DVAR. The analysis increment of v_winds, temperature, and non-dimensional pressure are like that of u_wind. The difference of analysis increment of the two systems over the Tibetan Plateau is not significant (Fig. 6c and 6d), it means that, over the Tibetan plateau, the horizontal localization scales between these two hybrid data assimilation systems have little difference. The above results show that the GRAPES-MESO En-3DVAR-TD-HLS scheme can achieve the result of the horizontal localization scale over the plain areas, which is smaller than that over the Tibetan Plateau.

Figure 7a and 7b illustrates the vertical profile of RMSE for analysis field of 3DVAR, GRAPES-MESO En-3DVAR and GRAPES-MESO En-3DVAR-TD-HLS data assimilation systems. The trend of the vertical profiles of these three data assimilation systems is basically similar. The maximum RMSE of u_wind and v_wind appeared in 200-300 hPa and top of the model layer. However, the RMSE of GRAPES-MESO En-3DVAR-TD-HLS is obviously less than that of 3DVAR and En-3DVAR at all levels. The RMSE of temperature and geopotential height differ slightly among these three data assimilation systems, so we will not discuss them in details.

Figure 8a and 8b is the vertical RMSE profile for 6h forecast of u_wind and v_wind, respectively, of the three data assimilation systems. Like the analysis fields in Fig. 7, the trend of the vertical RMSE profiles of the three data assimilation systems is basically the same. However, in Fig. 8, the difference in the RMSE between the three systems is reduced. Below 600 hPa level, the RMSE of GRAPES-MESO En-3DVAR-TD-HLS and 3DVAR are not much different, but it is slightly smaller than that of GRAPES-MESO En-3DVAR, while above 600 hPa

level, GRAPES-MESO En-3DVAR-TD-HLS is significantly better than the other two systems. Fig. 8c and 8d is the vertical RMSE profile for 12h forecast of u_wind and v_wind, respectively, of the three data assimilation systems. As can be seen, the differences in the RMSE between the three systems has been further reduced. Between 800 to 1,000 hPa, 3DVAR system is the smallest; above 800 hPa, the RMSE of GRAPES-MESO En-3DVAR-TD-HLS is significantly smaller than that of the other two systems; above 600 hPa, the 12h forecast results of both GRAPES-MESO En-3DVAR and GRAPES-MESO En-3DVAR-TD-HLS are better than that of 3DVAR. Overall, in the 6-24h forecasts, the RMSE of GRAPES-MESO En-3DVAR-TD-HLS are smaller than those of 3DVAR and GRAPES-MESO En-3DVAR. From 30 to 48h, these three data assimilation systems have similar results.

Figure 9 is the time series of total RMSE for 48h forecast of u_wind and v_wind of the three data

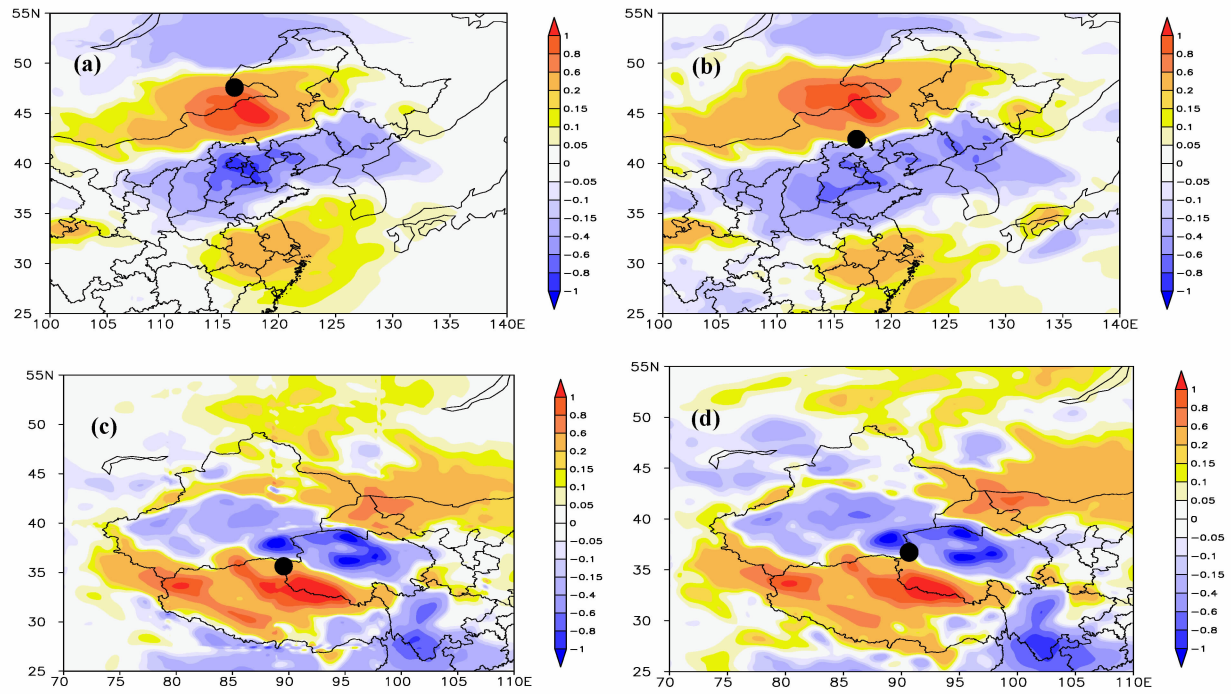

Figure 6. The results of the horizontal analysis increment of u_wind with a single-point pressure observation experiment over the plain (42°N, 117°E) and Tibetan Plateau (35°N, 90°E) with model level of 13. a) En-3DVAR-TD-HLS, b) En-3DVAR over the plain, c) En-3DVAR-TD-HLS and d) En-3DVAR over the Tibetan plateau.

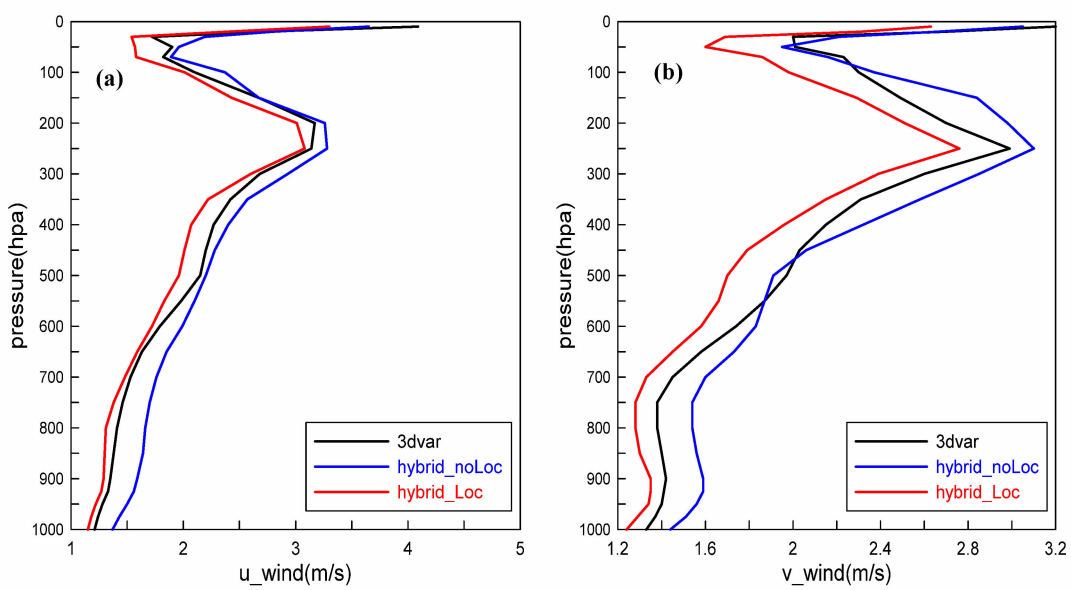

Figure 7. Vertical profile of RMS of analysis field, the black contour is 3DVAR system, the blue contour is hybrid_noLoc (GRAPES-MESO En-3DVAR), and the red contour is hybrid_Loc (GRAPES-MESO En-3DVAR-TD-HLS) . a) u_wind, b) v_wind.

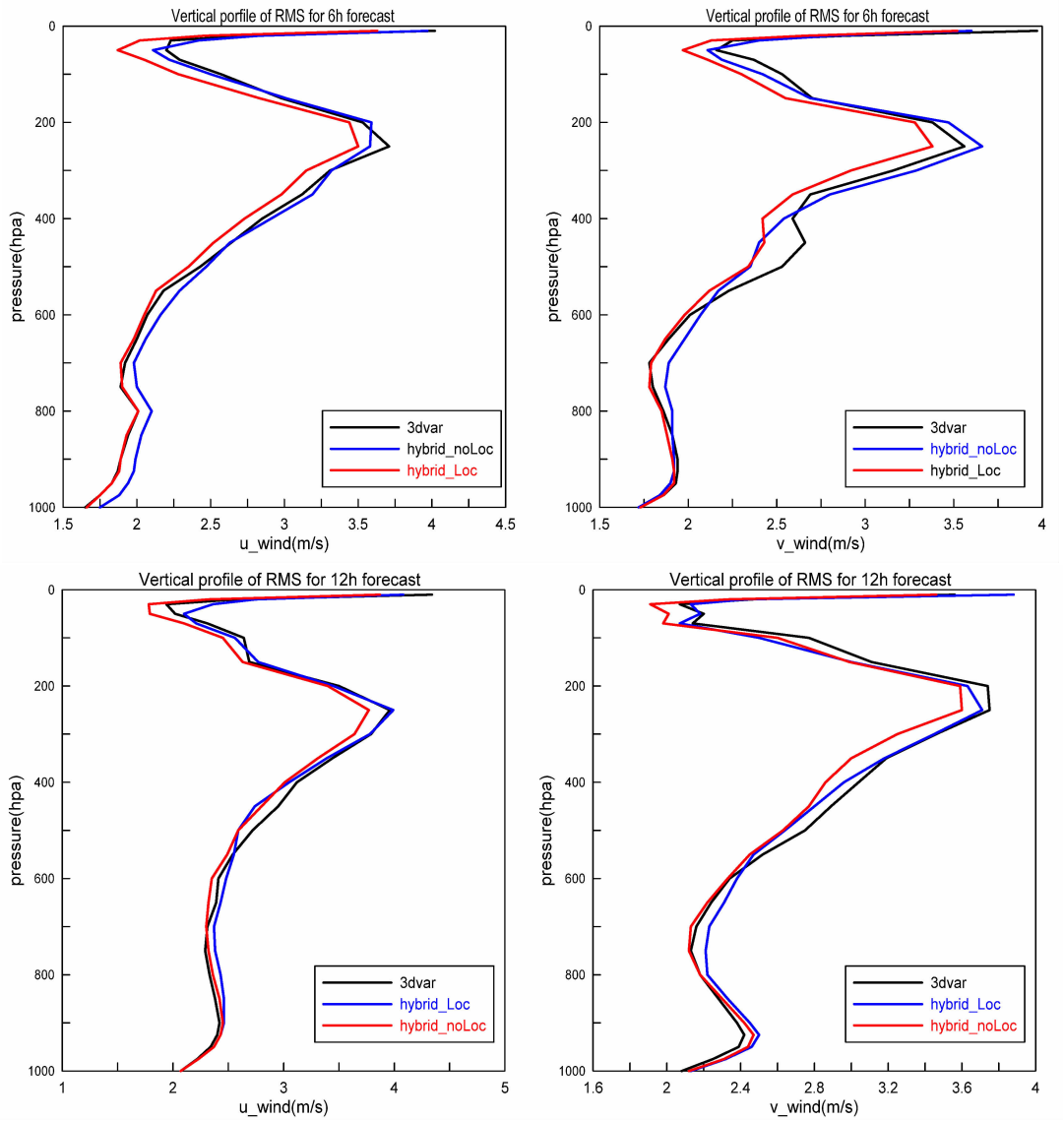

Figure 8. Vertical profile of RMS for 6h and 12h forecasts, the black contour is 3DVAR system, the blue contour is hybrid_noLoc (GRAPES-MESO En-3DVAR) , and the red contour is hybrid_Loc (GRAPES-MESO En-3DVAR-HLS_TC). Left panels: u_wind, right panels: v_wind.

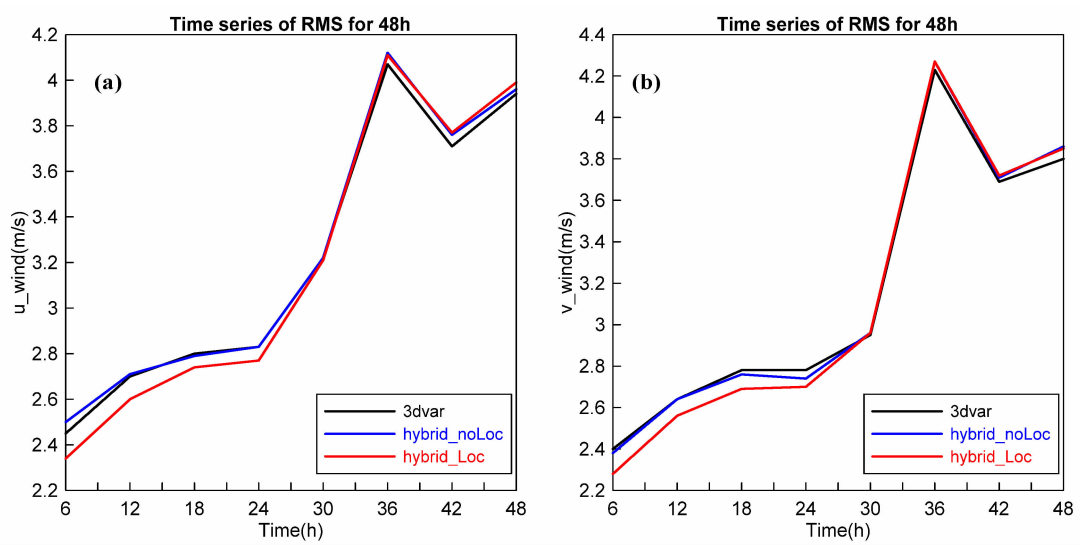

Figure 9. Time series of total RMS for 48h forecast, the black contour is 3DVAR system, the blue contour is hybrid_noLoc (GRAPES-MESO En-3DVAR), and the red contour is hybrid_Loc (GRAPES-MESO En-3DVAR-HLS_TC) . a) u_wind, b) v_wind.

assimilation systems. We can see that, in the 6-30h forecasting period, the forecast of GRAPES-MESO En-3DVAR-TD-HLS system is obviously better than that of the other two systems, with GRAPES-MESO En-3DVAR and 3DVAR having similar forecast skills. These three data assimilation schemes have the same result for the 36-48h forecasts.

The above experiments showed that the GRAPES-MESO En-3DVAR-TD-HLS system can improve the quality of GRAPES, and the topography-dependent horizontal localization scale method is reasonable and effective.

5 CONCLUSIONS

Based on the hybrid En-3DVAR assimilation system established by the National Meteorological Center, the 7-day simulations were conducted to obtain the optimal horizontal localization scale. With the results of 7-day simulations based on the GRAPES-MESO hybrid En-3DVAR assimilation system, we constructed a horizontal localization scale scheme which depends on topography. Data assimilation and forecast experiments of GRAPES-MESO En-3DVAR, 3DVAR and GRAPES-MESO En-3DVAR-TD-HLS have been conducted. The results are obtained as follows:

(1) The 7-day simulations results showed that over the Tibetan Plateau the optimal horizontal localization scale is 1,500 km, and over the plain area the optimal scale is 1,000 km. The reason for this result might be due to the data assimilation system needing a large horizontal localization scale to transfer the observation information to cover the Tibetan plateau, which have complex terrain and sparse observations.

(2) After constructing the topography-dependent horizontal localization scheme, we found that σ equaling to 100 satisfied the results of (1).

(3) Vertical profile of RMSE shows that the analysis field, for the 6h to 24h forecasting period, the GRAPES-MESO En-3DVAR-TD-HLS is better than that of the other two assimilation systems. In particular, the RMSE is significantly less than that of the other two systems across the vertical level in the analysis field.

(4) The time series of total RMSE for 48h forecast shows that, for the 6h to 30h forecasts, GRAPES-MESO En-3DVAR-TD-HLS is significantly better than the other two systems, with GRAPES-MESO En-3DVAR and 3DVAR having similar performance. The total RMSE of the three data assimilation systems in 36-48h is almost the same.

As an initial attempt to apply the topography-dependent horizontal localization scale method to the GRAPES-MESO En-3DVAR data assimilation system, we conducted some experiments by 3DVAR, GRAPES-MESO En-3DVAR, and GRAPES-MESO En-3DVAR-TD-HLS data assimilation system. Although GRAPES-MESO En-3DVAR-TD-HLS has some encouraging results with localization scale varying in horizontal direction, the horizontal localization scale changing with height needs to be considered in the future. In this paper, only conventional observations were used in these experiments, the unconventional observations, such as radar and satellite data will be implemented in our next study.

REFERENCES:

[1] PARRISH D F, DERBER J C. The national meteorological center's spectral statistical- interpolation analysis system [J]. Mon Wea Rev, 1992, 120(8): 1747-1763.

[2] RABIER F, THEPAUT J N, COURTIER P. Extend assimilation and forecast experiment with four-dimensional variational assimilation system [J]. Quart J Roy Meteor Soc, 1998, 124(550): 1861-1887.

[3] BARKER D M, HUANG W, GUO Y R, et al. A three-dimensional (3DVAR) data assimilation system for use with MM5: Implementation and initial result [J]. Mon Wea Rev, 2004, 132(4): 897-914.

[4] ANDERSON J L. An ensemble adjustment Kalman filter for data assimilation [J]. Mon Wea Rev, 2001, 129(12): 2884-2903.

[5] WHITAKER J S, HAMIL T M. Ensemble data assimilation without perturbed observation [J]. Mon Wea Rev, 2002, 130(7): 1913-1924.

[6] SNYDER C, ZHANG F. Test of an ensemble Kalman filter for convective-scale data assimilation [J]. Mon Wea Rev, 2003, 131(26): 1663-1677.

[7] TONG M, XUE M. Ensemble Kalman filter assimilation of Doppler radar data with a compressible non-hydrostatic model: OSS experiments [J]. Mon Wea Rev, 2005, 133(7): 1789-1807.

[8] ZHANG F, MENG Z, AKSOY A. Test of ensemble Kalman filter for mesoscale and regional scale data assimilation, Part I: Perfect-model experiment [J]. Mon Wea Rev, 2006, 134(2): 722-736.

[9] TORN R D, HAKIM G J, SNYDER C. Boundary conditions for a limited-area ensemble Kalman filter [J]. Mon Wea Rev, 2006, 134(9): 2490-2502.

[10] MENG Z, ZHANG F. Test of ensemble Kalman filter for mesoscale and regional scale data assimilation, Part II: Imperfect-model experiments [J]. Mon Wea Rev, 2007, 135(4): 1403-1423.

[11] ZHANG F, WENG Y, SIPPEL J A, et al. Cloud-resolving hurricane initialization and prediction through assimilation of Doppler radar observations with an Ensemble Kalman Filter [J]. Mon Wea Rev, 2009, 137 (7): 2105-2125.

[12] HAMILL T M, SNYDER C, MORSS R E. Analysis-error statistics of a quasi-geostrophic model using three-dimensional variational assimilation [J]. Mon Wea Rev, 2002, 130(11): 2777-2790.

[13] WANG X. Incorporating ensemble covariance in the Gridpoint Statistical Interpolation (GSI) variational minimization: A mathematical framework [J]. Mon Wea Rev, 2010, 138(7): 2990-2995.

[14] WANG X, PARRISH D, KLEIST D, et al. GSI 3DVAR-based ensemble-variational hybrid data assimilation for NCEP global forecast system:

single-resolution experiments [J]. Mon Wea Rev, 2013, 141(11): 4098-4117.
[15] WANG X, BARKER D, SNYDER C, et al. A hybrid ETKF-3DVAR data assimilation scheme for the WRF model, Part I: Observing system simulation experiment [J]. Mon Wea Rev, 2008, 136 (12): 5116-5131.
[16] WANG X. Application of the WRF hybrid ETKF-3DVAR data assimilation system for hurricane track forecasts [J]. Wea Forecast, 2011, 26(6): 868-884.
[17] WANG X, BARKER D, SNYDER C, et al. A hybrid ETKF-3DVAR data assimilation scheme for the WRF model, Part II: Real observation experiments [J]. Mon Wea Rev, 2008, 136(12): 5132-5147.
[18] CLAYTON A M, LORENC A C, BARKER D M. Operational implementation of a hybrid ensemble/4D-Var global data assimilation system at the Met Office [J]. Quart J Roy Meteor Soc, 2012, 39(675): 1445-1461.
[19] COURTIER P, ANDERSSON E, HECKLEY W A, et al.. The ECMWF implementation of three-dimensional variational assimilation (3DVAR), Part I: Formulation [J]. Quart J Roy Meteor Soc, 1998, 124(550): 1783-1807.
[20] BUEHNER M. Ensemble-derived stationary and flow dependent background error covariances: Evaluation in a quasi-operational NWP setting [J]. Quart J Roy Meteor Soc, 2005, 131(607): 1013-1043.
[21] WANG X, C SNYDER, HAMILL T M. On the theoretical equivalence of differently proposed ensemble/VAR hybrid analysis schemes [J]. Mon Wea Rev, 2007, 135(1): 222-227.
[22] HAMILL T M, SNYDER C. A hybrid ensemble Kalman filter-3D variational analysis scheme [J]. Mon Wea Rev, 2000, 128(8): 2905-2919.
[23] HAMILL T M, WHITAKER J S, FIORINO M, et al. Global ensemble predictions of 2009's tropical cyclones initialized with an ensemble Kalman filter [J]. Mon Wea Rev, 2011, 139(2): 668-688.
[24] HAMILL T M, WHITAKER J S, et al. Predictions of 2010's tropical cyclones using the GFS and ensemble-based data assimilation methods [J]. Mon Wea Rev, 2011, 139(10): 3243-3247.
[25] LORENC A C. The potential of the ensemble Kalman filter for NWP-a comparison with 4D-VAR [J]. Quart J Roy Meteor Soc, 2003, 129(595): 3183-3203.
[26] BUEHNER M. Ensemble-derived stationary and flow dependent background error covariances: Evaluation in a quasi-operational NWP setting [J]. Quart J Roy Meteor Soc, 2005, 131(607): 1013-1043.
[27] WANG X, SNYDER C, HAMILL T M. On the theoretical equivalence of differently proposed ensemble/VAR hybrid analysis schemes [J]. Mon Wea Rev, 2007, 135(1): 222-227.
[28] LIU C, XIAO Q, WANG B. An ensemble-based four-dimensional variational data assimilation scheme, Part II: Observing System Simulation Experiments with advanced research WRF (ARW) [J]. Mon Wea Rev, 2009, 137(5): 1687-1704.
[29] LIU C, XIAO Q. An ensemble-based four-dimensional variational data assimilation scheme, Part III: Antarctic applications with advanced research WRF using real data [J]. Mon Wea Rev, 2013, 141(8): 2721-2739.
[30] BUEHNER M, HOUTEKAMER P L, CHARETTE C, et al. Inter-comparison of variational data assimilation and ensemble Kalman filter for global deterministic NWP, Part I: Description and single-observation experiments [J]. Mon Wea Rev, 2010, 138 (5): 1550-1566.
[31] BUEHNER M, HOUTEKAMER P L, CHARETTE C, et al. Inter-comparison of variational data assimilation and ensemble Kalman filter for global deterministic NWP, Part I: One-month experiments with real observations [J]. Mon Wea Rev, 2010, 138(6): 1567-1586.
[32] MA Xu-lin, LU Xu, YU Yue-ming, et al. Progress on hybrid ensemble-variational data assimilation numerical weather prediction [J]. J Trop Meteor, 2014, 30 (6): 1118-1195 (in Chinese).
[33] MA Xu-lin, LI Lin-lin, ZHOU Bo-yang, et al. Flow-dependent characteristics of typhoon forecasting errors and optimal coupling coefficient in hybrid data assimilation [J]. Trans Atmos Sci, 2015, 38(6): 766-775 (in Chinese).
[34] ZHANG Ming-yang, ZHANG Li-feng, ZHANG Bin, et al. Flow-dependent characteristics of background error covariance in hybrid variational-ensemble data assimilation [J]. J Meteor Sci, 2015, 35(6): 728-736.
[35] ZHU Hao-nan, MIN Jin-zhong, DU Ning-zhu, et al. Implementation and testing of a hybrid back and forth nudging ensemble Kalman filter (HBFNEnKF) data assimilation method [J]. Chin J Atmos Sci, 2016, 40(5): 995-1008 (in Chinese).
[36] SHEN Fei-fei, MIN Jin-zhong, XU Dong-mei, et al. Assimilation of Doppler radar velocity observations with hybrid ETKF-3DVAR method, Part I: Experiments with simulated data [J]. Trans Atmos Sci, 2016, 39(1): 81-89 (in Chinese).
[37] CHEN Liang-lv, CHEN Jing, XUE Ji-shan, et al. Development and testing of the GRAPES regional ensemble-3DVAR hybrid data assimilation system [J]. J Meteor Res, 2015, 29(6): 981-996 (in Chinese).
[38] ZHANG Han-bin, CHEN Jing, ZHI Xie-fei, et al. Study on the Application of GRAPES Regional Ensemble Prediction System [J]. Meteor Mon, 2014, 40 (9): 1076-1085 (in Chinese).
[39] ZHANG Han-bin, ZHI Xie-fei, CHEN Jing, et al. Study of the modification of multi-model ensemble scheme for tropical cyclone forecast [J]. J Trop Meteor, 2015, 21(4): 389-399.
[40] ZHANG Han-bin, CHEN Jing, ZHI Xie-fei, et al. Design and comparison of perturbation schemes for GRAPES_Meso based ensemble forecast [J]. Trans Atmos Sci, 2014, 37(3): 276-384 (in Chinese).
[41] HOUTEKAMER P L, MITCHELL H L. Data assimilation using an ensemble Kalman filter technique [J]. Mon Wea Rev, 1998, 126(3): 796-811.
[42] HOUTEKAMER P L, MITCHELL H L. A sequential ensemble Kalman filter for atmospheric data assimilation [J]. Mon Wea Rev, 2001, 129(1): 123-137.
[43] GASPARI G, COHN S. Construction of correlation functions in two and three dimensions [J]. Quart J Roy Meteor Soc, 1999, 125(554): 723-757.
[44] OTT E, HUNT B R, SZUNYOGH I, et al. Exploiting local low dimensionality of the atmospheric dynamics for efficient ensemble Kalman filtering [R]. San Francisco: American Geophysical Union, 2002: 12.

[45] OTT E, HUNT B R, SZUNYOGH I, et al. A local ensemble Kalman filter for atmospheric data assimilation [J]. Tellus, 2004, 56(A): 415-428.

[46] HUNT B R, KOSTELICH E J, SZUNYOGH I. Efficient data assimilation for spatiotemporal chaos: A local ensemble transform Kalman filter [J]. Physical Data-an, 2007, 230(1-2): 112-126.

[47] MIYOSHI T, YAMANE S, ENOMOTO T. Localizing the error covariance by physical distances within a local ensemble transform Kalman filter (LETKF) [J]. SOLA, 2007, 3(27): 89-92.

[48] SZUNYOGH I, KOSTELICH E J, GYARMATI G, et al. A local ensemble transform Kalman filter data assimilation system for the NCEP global model [J]. Tellus, 2008, 60(A): 113-130.

[49] LIU Shuo, MIN Jin-zhong. The study of adaptive localization and adaptive covariance inflation for WRF-EnSRF Assimilation System [D]. Nanjing: Nanjing University of Information Science & Technology, 2012.

Citation: XIA Yu, CHEN Jing, ZHI Xie-fei, et al. Topography-dependent horizontal localization scale scheme in GRAPES-MESO hybrid En-3DVAR assimilation system [J]. J Trop Meteor, 2019, 25(2): 245-256.